Development of doped ZnO-based biomimicking and tumor targeted nanotheranostics to improve pancreatic cancer treatment

Sugata Barui
Politecnico di Torino
Nicolò Maria Percivalle
Politecnico di Torino
Marzia Conte
Politecnico di Torino
Bianca Dumontel
Politecnico di Torino
Luisa Racca
Politecnico di Torino
Marco Carofiglio
Politecnico di Torino
Valentina Cauda (valentina.cauda@polito.it)
Politecnico di Torino

Research Article

Keywords: Doped Zinc Oxide nanocrystal, Extracellular vesicles, Targeted Nanotheranostics, Pancreatic cancer, Magnetic resonance imaging, Gemcitabine

Posted Date: June 21st, 2022

DOI: https://doi.org/10.21203/rs.3.rs-1738921/v1

Abstract

Despite different nanomaterials were developed so far against cancer, their potential drawbacks are still scarcely considered. The off-target delivery of a therapeutic compound, as well as the non-specific uptake of these nanomaterials by healthy tissues or organs, and their potential immunogenicity are some of the major issues that still have to be faced prior to a successful clinical translation.

This work aims to develop an innovative theranostic, biocompatible, and drug-loaded nanoconstruct based on Gadolinium-doped Zinc Oxide nanocrystals (Gd-ZnO NCs), focusing on one of the most lethal diseases, i.e. pancreatic cancer. The use of ZnO is motivated by the huge potential of this nanomaterial already demonstrated for in vitro and in vivo applications, while the Gadolinium doping confers magnetic properties useful for diagnostics. Furthermore, an innovative biomimetic shell is here used to coat the NCs: it is composed of a lipid bilayer made from extracellular vesicles (EVs) combined with other synthetic lipids and a peptide targeting the pancreatic tumor microenvironment. To complete the nanoconstruct therapeutic function, Gemcitabine, a first line drug for pancreatic cancer treatment, was adsorbed on the Gd-doped NCs prior to the coating with the above-mentioned lipidic shell. The aim of this work is thus to strongly enhance the therapeutic capability of the final nanoconstruct, providing it with high biocompatibility, colloidal stability in biological media, efficient cargo loading and release properties, as well as active targeting for site selective drug delivery. Furthermore, the magnetic properties of the Gd-doped ZnO core can in future allow efficient in-situ bioimaging capabilities based on Magnetic Resonance Imaging technique.

The obtained nanoconstructs were tested on two different pancreatic cancer cell lines, i.e. BxPC-3 and the metastatic AsPC-1, proving high cell internalization levels, mediated by the targeting peptide exposed on the nanoconstruct. Cellular cytotoxicity assay performed on both cell lines dictated ~20% increased cell killing efficacy of Gemcitabine when delivered through the nanoconstruct rather than as a free drug. Taken together, our designed theranostic nanoconstruct can have a significant impact on the standard treatment of pancreatic cancer.

Introduction

Pancreatic cancer (PC) is nowadays one of the deadliest existent tumours, accounting for about 3% of all cancers and about 7% of all cancer deaths in the US(1). In particular, pancreatic ductal adenocarcinoma (PDAC) makes up over 90% of the total number of PC cases(2). The hallmarks of PDAC are (I) the presence of genetic alterations(3); (II) disrupted molecular pathways(4); (III) tumour plasticity and heterogeneity(5); (IV) desmoplastic, hypoxic and immunosuppressive tumour microenvironment (TME), commonly referred to as tumour stroma(6–8); (V) metastasis formation(9) and (VI) therapy resistance(10). Its late diagnosis, often made when the primary tumour is locally unresectable or metastases are already spread throughout the body(11), is mainly responsible for the low overall median survival and 5-year survival rate of patients(12), who in turn are usually faced with limited alternatives in terms of curative treatments.

Currently, surgery followed by adjuvant therapy(13) or preceded by neoadjuvant therapy(14, 15) is the main route for resectable and locally advanced PDAC, while most unresectable and metastatic tumours are treated with palliative chemotherapy, since other treatments such as radiotherapy, chemoradiation and chemotherapy followed by radiotherapy have been proved to be rather unsuccessful(16).

Over the last few decades, several chemotherapeutic agents have been considered for first and second-line therapies: 5-fluorouracil(17), Gemcitabine(18) and its combination with other cytotoxic and biological agents(19–23), the multidrug regimen FOLFIRINOX(24, 25), nab-Paclitaxel (also known as Abraxane) in combination with Gemcitabine(26). However, none of them succeeded in remarkably improving patients' survival and the incidence of several adverse effects resulting in drug resistance and high toxicity have been reported so far(17, 25, 27, 28). In order to overcome these limitations, other strategies such as anti-angiogenic therapies(29), targeted therapies(30) and stroma targeting(31) have been carried out, still with limited success mainly due to the difficulty of therapeutic agents in penetrating the TME. In fact, tumour stroma contributes to an increased interstitial fluid pressure (IFP)(32), which in turn results in collapsed blood vessels(33) and impaired drug delivery(34).

Therefore, implementing more efficient systems to achieve a better intratumoral delivery of therapeutics and to overcome drug resistance is an urgent need which has been increasingly addressed thanks to recent nanomedicine advances(35–37).

Gemcitabine is still considered the gold standard first-line single drug treatment against PDAC, however chemoresistance(38, 39) and metabolic clearance(40) rapidly occur in patients after some administered cycles. For these reasons, many platforms have been implemented in order to enhance its delivery, such as liposomes, nanogels and micelles. Nevertheless, poor loading efficiency and low structural stability are the main issues related to their use(41).

Thanks to their high surface/volume ratio, their versatility, their optical properties and their manifold custom-build possibilities, nanoparticles (NPs) have been recently considered as drug carriers(42). Indeed, they can protect the cargo and ensure a better tumour delivery, enhancing the response to chemotherapy; moreover, the incorporation of targeting agents allow NPs to reach the tumour area in a selective way, sparing healthy cells and thus minimizing toxicity towards them(43).

Furthermore, inorganic NPs can be used for imaging purposes, i.e. as MRI contrast agents, ultimately fulfilling their theranostic capabilities by allowing their tracking and tumour accumulation(44, 45). The main drawbacks related to their application are their low biostability in biological media, their tendency to aggregate and their low biocompatibility. To overcome these issues, NPs shielding with lipidic bilayers has been proposed as a promising strategy, able to mimic cell membranes and to avoid the immunological response(46). Among the many inorganic nanoparticles suitable for cancer therapy, zinc oxide nanocrystals (ZnO-NCs) have emerged thanks to their biocompatibility, piezoelectric properties(47) and cytotoxicity mechanisms preferably affecting cancer cells (mainly based on ROS generation and Zn^{2+} ions release)(48). To enhance their biostability, coatings made of commercially available lipids have

been successfully applied on their surface and tested within different anticancer applications(49–51). Moreover, to further improve their biomimicry and confer them tumour homing and membrane crossing abilities, the use of extracellular vesicles (EVs) as drug delivery systems has recently been proposed(52–54) and successfully applied by our group to stabilize the ZnO-NCs in biological environment and increase their internalization in cancer cells, obtaining low immunogenic nanoplatforms with customizable targeting abilities(55, 56).

In the present work, the development of an innovative theranostic non-immunogenic nanoconstruct against PDAC is proposed. A core of oleic acid stabilized ZnO-NCs, doped with a rare earth element, i.e. Gadolinium, for imaging purposes(57), is loaded with Gemcitabine by physical adsorption and coated by means of the freeze thaw technique with a hybrid lipidic shell, consisting of EVs and commercially available lipids conjugated to a targeting peptide (CKAAKN), which specifically targets both the pancreatic cancer cells and the angiogenic vessels of the tumor microenvironment (i.e. the Wnt-2 pathway)(58). To achieve the final nanoconstruct, a series of optimizations of process parameters and freeze-thaw protocols are implemented and supported by a thorough characterization in terms of chemical composition, dimension, surface properties, aggregation in water-based media and achieved colocalization of the single components. The optimized nanoconstruct is validated on two human-derived PDAC cell lines, BxPC-3 and the metastatic AsPC-1 aiming to obtain a remarkable cytotoxic effect on cells, with respect to the same nanoconstruct without drug and to Gemcitabine alone. Moreover, the presence of the targeting peptide is expected to enhance the cell uptake of the nanoconstruct.

The proposed drug-loaded nanoconstruct paves the way for an innovative, biomimetic, site-selective and theranostic nanotool, able to improve Gemcitabine activity and induce apoptosis of pancreatic cancer cells(59), certainly deserving future investigations in vitro 3D models, organ-on-chips and in vivo analysis.

Materials And Methods

Nanomaterial synthesis and chemical functionalization

For the synthesis of Gd-doped, oleate-stabilized Zinc Oxide nanocrystals (Ol-ZnO-Gd NCs), 0.5268 g of zinc acetate dihydrate ($Zn(CH_3COO)_2{\cdot}2H_2O$, 2.4 mmol from Sigma-Aldrich), stored in dry conditions under vacuum, were dissolved in 40 ml of ethanol in a 100 ml round-bottom flask together with 0.0963 g of Gadolinium(III) acetate hydrate ($Gd(CH_3COO)_3{\cdot}H_2O$, 0.287 mmol from Sigma-Aldrich) to obtain the desired molar ratio of zinc precursor and the dopant, which was equal to 1:0.12. Then 140 µl of oleic acid (≥ 99%, Sigma-Aldrich) was added and the obtained solution was heated at 70°C on a stirring plate (VELP Scientifica ARE Hot plate stirrer) at 350 rpm using a heating silicone oil bath, after closing the flask with a refrigerating column. After complete precursors dissolution (after around 3 minutes), a solution made by 0.522 g of TMAH (Tetramethylammonium hydroxide, 98.5%, Sigma-Aldrich) dissolved in 1.052 ml of bidistilled water (obtained by a Direct Q3 system, Millipore) and 10 ml of ethanol was prepared and added to the flask, turning the colloidal solution from transparent to white. After 15 minutes, the reaction was stopped by placing the flask in an ice bath and rapidly adding 40 ml of ice-cold (0–4°C) ethanol. The

nanocrystals suspension was then centrifuged for 5 minutes at 10000 RCF, the reaction supernatant discarded, and 30 ml of fresh ethanol added to redisperse the nanocrystals through a vortex stirrer and an ultrasound bath. Finally, two washing steps with ethanol were performed through the succession of centrifugation and resuspension steps by sonication and vortex.

As a control, pristine, oleate-stabilized Zinc Oxide nanocrystals (Ol-ZnO NCs) were synthesized following the same procedure without the addition of Gd acetate hydrate. In this case, the reaction was carried out for 5 minutes (instead of 15 as in the case of the doped NCs).

The synthetized NCs were also functionalized with amino-propyl groups. The functionalization process was implemented taking the volume corresponding to 40 mg of nanocrystals from the stock and putting it in the round bottom flask, where the amount of ethanol needed to reach a final concentration of 2.5 mg/ml was previously added. Then, the flask was immersed in a silicone oil bath at 70°C, closed with a refrigerating column with sealing grease and nitrogen gas was flowed to strip out humidity. When the condensation in the flask started, 12.5 µl of APTMS (3-Aminopropyl)trimethoxysilane, 0.0716 mmol, Sigma-Aldrich) was added, corresponding to 14.5% with respect to the moles of ZnO NCs. The whole procedure lasted 6 hours and when the final suspension cooled down, it was collected by centrifugation for 10 minutes at 10000 RCF and resuspended in 5 ml of fresh ethanol through sonication. Finally, two washing steps in ethanol were performed.

Nanocrystals characterization

Field Emission Scanning Electron Microscopy (FESEM) measurements were carried out using a FESEM Merlin (from Zeiss) coupled with X-Ray detector for EDS Analysis. For the samples' preparation, an ethanol-diluted aliquot of the nanocrystals' solution was put dropwise on top of a silicon wafer.

A DC magnetometer (Lake Shore 7225, Lake Shore Cryotronics, Inc.) equipped with a cryogen-free magnet system was used to examine the magnetic properties of the Gd-doped NCs compared to the undoped ones. Measurements were performed at room temperature in quasistatic condition for 1 mg of both doped and undoped NCs.

Dynamic Light Scattering (DLS) and Zeta potential measurements (both in ethanol and water) were performed with the Zetasizer Nano ZS90 (Malvern Instruments). The samples were first sonicated for 10 minutes and 100 µg of NCs was used for each measurement. Each sample (final concentration of 100 µg/ml) was then sonicated, vortexed and put in a 1 ml cuvette (DTS0012), and the DLS Size measurements in both ethanol and water were performed. Then, 750 µl of the sample in water was put in another cuvette (DTS1070) for Zeta potential measurements.

Drug adsorption

Gemcitabine (Gemcitabine hydrochloride, Sigma-Aldrich) uptake analysis was performed with the UV-Vis spectrophotometer (Multiskan FC, Thermo Scientific), coupled with the Thermo Scientific Skan-it Software for data collection.

Gemcitabine calibration curve in water was derived through serial dilutions starting from a 1 mM concentrated drug stock (1 mM, 100 µM, 10 µM, 0.1 µM) and measuring the absorbance values at a wavelength of 272 nm. The next step was to identify the time necessary to obtain an optimal adsorption of the drug on the NCs' surface. To this end, the volume corresponding to 200 µg of amine-functionalized NCs was put into different 1.5 ml tubes, one for each time step (2 h, 3 h, 4 h, 6 h), and centrifuged at 14000 RCF for 10 minutes. The pellets were resuspended in 400 µl of drug at 1 mM concentration (in bidistilled water) and samples were put on a magnetic stirring plate (200 rpm). Two additional samples were prepared as controls: the drug's solvent (negative control, bidistilled water without drug), and the 1 mM drug solution (positive control). At each time step, the corresponding sample was centrifuged (14000 RCF, 10 min), and three replicates of 100 µl of the supernatant were put in a synthetic quartz glass (QG)96 wells plate (Hellma Analytics), together with the controls, and analyzed with the UV-Vis spectrophotometer. The absorbance value of the negative control was subtracted to the absorbance values of the other samples. Then, the drug's concentration in the samples was derived using the equation of the calibration curve, and the concentration of drug adsorbed on the NCs' surface was obtained by subtracting the molarity of the sample to the one related to the positive control.

Extracellular vesicles and lipid coating

The nanoconstruct coating was obtained using extracellular vesicles (EVs), derived from healthy B lymphocytes (IST-EBV-TW6B purchased from IRCCS AOU San Martino IST), and commercially available lipids to whom the targeting peptide CKAAKN was bound. Liposomes, EVs, and drug-loaded nanocrystals were separately prepared and the NCs' encapsulation in the lipidic shell was obtained through the freeze-thaw technique in liquid nitrogen.

Targeted liposomes, henceforward called Lipo-pep, were formed by DOPC (1,2-dioleoyl-sn-glycero-3-phosphocholine from Avanti Polar Lipids Inc.) and DSPE-PEG(2000)Maleimide (Avanti Polar Lipids Inc.) coupled with CKAAKN synthetic peptide. First, a lipids' stock was prepared: the volume corresponding to 2.5 mg of DOPC was dried to evaporate chloroform and then 400 µl of ethanol and 600 µl of bidistilled water were added obtaining a concentration of 2.5 mg/ml. Ethanol was added to prevent the formation of liposomes in the stock already.

Starting from this stock, Lipo-pep were prepared exploiting a solvent-exchange method(49, 60), diluting DOPC lipids 1:10 in bidistilled water. The complex of DSPE-PEG(2000)-maleimide and CKAAKN-peptide (molar ratio 3:1) was obtained dissolving the two components in dimethylsulfoxide (DMF, Sigma-Aldrich) at 37.5 and 50 mM, respectively. The peptide solution was diluted in 0.1 M sodium phosphate buffer (pH 7.4) and DSPE-PEG(2000)-maleimide was then added to the mixture obtaining a final reaction mixture of 1:1 DMF/(sodium phosphate buffer) with 5 mM peptide and 15 mM DSPE-PEG(2000)-maleimide. The reaction was allowed to proceed for 1 h at room temperature. Then, it was kept at -20°C and used as a stock. The so obtained DSPE-PEG(2000)-CKAAKN lipids, henceforward called functional lipids, were added to the already formed DOPC liposomes (Lipo) in the molar ratio of 99.5:0.5 mol% (Lipo:functional lipids). Considering 25 µl of DOPC lipids from the stock (2.5 mg/ml), the corresponding moles of

functional lipids were calculated, equal to 0.0004 µmol. Accordingly, the needed volume of functional lipids (whose stock was at a concentration of 17.87 mg/ml) was calculated (0.08 µl).

Once prepared, the Lipo-pep solution was incubated into an orbital shaker (VWR Incubating orbital shaker, Professional 3500) for 8 h at 37°C and 200 rpm in order to stabilize the liposomes' structure and allow the incorporation of functional lipid in the DOPC lipidic shell. Finally, a dialysis process was performed to remove the unbound peptide using a dialysis membrane (SnakeSkin dialysis Tubing 3.5K MWCO, 16 mm dry I.D., 35 feet by Thermofisher Scientific) against bidistilled water at the ratio of 1 l of water for 1 ml of Lipo-pep solution, at 80 rpm for 18 hours.

EVs were isolated from conditioned cell culture supernatants of B lymphocytes according to an ultracentrifugation protocol, as previously reported(61), and stored at -80°C in aliquots of 50 µl in 0.9% NaCl solution. The freeze-thaw technique, which consists in the alternation of a freezing of the sample in liquid nitrogen (-196°C) and a following thawing at room temperature, was exploited to coat the nanocrystal with the lipidic shell in a ratio of 1:0.125:0.5 (µg of protein content of EVs, µg of Lipo-pep, and µg of nanocrystals respectively).

Briefly, the Lipo-pep stock was sonicated for 1 minute and vortexed, before putting the required volume into a cryovial. Then, the pellet of the previously Gemcitabine-loaded NCs (stored at − 20°C overnight after the drug uptake) was redispersed in bidistilled water (concentration 10 µg/µl) through vigorous mixing, and the volume needed to obtain the desired ratio was added in the vial. The desired amount of thawed EVs (measured from the µg of proteins quantified by Bradford Assay) was concentrated through a 50 kDa Amicon filter (Sigma-Aldrich), at 14000 RCF for 10 minutes to remove the solution in excess. The final volumes of EVs in NaCl solution and drug-loaded NCs + Lipo-pep in bidistilled water was then adjusted to be in a ratio of 1:1 before mixing.

Then, 6 freeze-thaw cycles (3 minutes of freezing in liquid nitrogen followed by a thawing of 15 minutes) were performed, followed by 1 h of incubation in the orbital shaker (37°C, 200 rpm). At the end of the process, schematized in Fig. 1, the obtained final nanoconstruct was named as EV-Lipo-pep-NCs-Gem. The same nanoconstruct without loaded drug on the NCs surface (EV-Lipo-pep-NCs) was developed to characterize the preparation process and tested in terms of cellular uptake and cells viability, as control, to evaluate the nanoconstruct safety in absence of Gemcitabine.

Nanoconstruct characterization

DLS Size and Zeta potential measurements were performed as above on the nanoconstruct, as well as Nanoparticle Tracking Analysis (NTA), using the NanoSight NS300 from Malvern Panalytical. 50 µl of the nanoconstruct suspension was diluted 1:10 in a 1:1 solution of 0.1 µm filtered bidistilled water and 0.1 µm filtered 0.9% NaCl solution and filled in the instrument microfluidic chamber. The detection was carried out by a λ = 505 nm laser beam and 20x magnification objective. Three videos of 60 s were captured for each sample, each with an infusion rate of 50 and a camera level between 11 and 16. Videos were analyzed with the NTA 3.2 software, setting the detection threshold at 5.

Transmission Electron Microscopy (TEM) analyses were carried out using a Thermo Scientific Talos™ F200X G2 S(TEM) operating at 60 kV. For these measurements, performed without staining the sample, the freshly prepared EV-Lipo-pep-NCs nanoconstruct was diluted at a final concentration of 10 µg/ml in 1:1 bidistilled water and NaCl solution. Then, a single drop of the diluted sample was put on a copper holey carbon grid and let dry before being analyzed.

Fluorescence microscopy analyses were performed to assess the NCs co-localization with the lipidic shell; for these measurements, a wide-field fluorescence inverted microscope (Nikon Eclipse Ti-E), operating with the NIS-element software, equipped with a super bright wide-spectrum source (Shutter Lambda XL) and a high-resolution camera (Zyla 4.2 Plus, 4098×3264 pixels, Andor Technology) was exploited, using a 60x and a 100x immersion oil objective (Plan Apo 1.40, Nikon). The different components of the nanoconstruct were labeled as follows: the aminopropyl-functionalized NCs with Atto 550 NHS ester (excitation peak at 544 nm, emission peak at 576 nm, Sigma-Aldrich), the peptide-lipid conjugate with FITC (excitation peak at 495 nm, emission peak at 519 nm); EVs with WGA647 (Wheat Germ Agglutinin - Alexa FluorTM 647 Conjugate, Thermo Fisher, excitation peak at 650 nm, emission peak at 668 nm). For the NCs labeling, Atto 550 NHS ester (Sigma Aldrich) was added in the ratio of 1 µl per 500 µg of NCs and overnight stirred at 200 rpm. Then, the sample was centrifuged for 10 minutes at 14000 RCF and washed twice with ethanol. The pellet was dispersed in bidistilled water (concentration 10 µg/µl), and this new stock was used for the nanoconstruct preparation. Concerning the Lipo-pep labeling, the CKAAKN peptide already bound to FITC dye (BioFab) was ad-hoc prepared and bound to the functional lipid, obtaining DSPE-PEG-CKAAKN-FITC, then used to prepare the Lipo-Pep formulation. Finally, the stock 50 µl solution of EVs in the cryovials were double diluted with the addition of physiological solution, and 1 µl of WGA647 was added, orbitally shaken (37°C, 200 rpm) for 30 minutes, and then purified with 50 kDa Amicon filter to remove unbound dye.

Once all the nanoconstruct components were labeled, the coupling process was carried out by freeze-thaw method, as reported above. The fluorescence microscope analysis was carried out diluting the sample 1:20 in bidistilled water and 2 µl of the diluted solution was put onto a microscope slide, sheltered with a cover glass slip, and analyzed. The encapsulation's efficacy was evaluated using the colocalization tool of the NIS software (Nikon): after setting a threshold between 0.1 and 1 µm (to exclude large aggregates), the spots in the 3 channels (the red one to visualize the NCs, the green one to visualize the liposomes, and the far-red one to visualize the EVs) and the overlapped spots in the merged images were counted. The successful coupling was measured on the ATTO 550-labeled NCs colocalized with the other channels, thus using the following equation: %colocalized NCs = (n◦ colocalized red spots)/(tot n◦ red spots).

Drug release

To assess the Gemcitabine release, RPMI 1640 cell culture medium (ATCC) supplemented by 10%v of Fetal Bovine Serum (ATCC) was used as dispersant and the drug release kinetics was compared between the lipid-coated NCs with respect to the uncoated ones. The volume corresponding to 350 µg of aminopropyl functionalized Ol-ZnO-Gd NCs was taken in quadruplicates from the stock and centrifuged

at 14000 RCF for 10 minutes into four different 1.5 ml tubes. Two of the pellets were resuspended in 700 µl of Gemcitabine 1 mM water solution, while the other two were dispersed in 700 µl of bidistilled water. Drug uptake was then carried out at 200 rpm for 2 h. Then, the samples were centrifuged at 14000 RCF for 10 minutes, and the supernatant was analyzed by UV-Vis spectroscopy to verify the successful adsorption of the drug. The four pellets were then put at -20°C. After 18 hours, two of the pellets (one drug-loaded NCs and one without drug as control) were thawed and coated only with liposomes in the ratio of 0.25:0.125:0.5 (µg of Lipo, µg of Lipo-pep, and µg of NCs respectively), resulting in Lipo-Lipo-pep-NCs nanoconstructs (see Supporting Information for the detailed preparation). Once prepared, these two samples were centrifuged at 10000 RCF for 5 minutes, and the supernatant was thrown away. Then, the other two samples (one drug-loaded NCs and one drug-unloaded, as control, both without lipid coating) were also thawed and all the four pellets were resuspended in 700 µl of cell culture medium. To obtain technical triplicates for each group, 600 µl from each sample were equally split (i.e. 200 µl) into three 1.5 ml tubes, filled with 800 µl of RPMI 1640, in order to reach the concentration of 100 µg/ml. Furthermore, 1 ml of medium was also prepared in triplicate as a blank control.

All the 15 samples were orbitally shaken at 37°C and 200 rpm, and the drug release was monitored after 0.5, 2, 24, 48, 72 and 96 hours. At each time step, samples were centrifuged at 10000 RCF for 5 minutes and the supernatant of each sample was analyzed in triplicate using a quartz microplate to measure UV-Vis absorbance. The pelleted particles were then dispersed, through vigorous mixing, in the remaining supernatant and the samples were put back in the orbital shaker. After the absorbance readings, the analyzed supernatants were put back in each tube to continue the drug release experiment.

To evaluate the amount of drug released after each time step a calibration curve was used and the absorbance value of the blank medium control was subtracted to the one of all the other samples; furthermore, the remaining absorbance value of the NCs and Lipo-Lipo-pep-NCs control samples was also subtracted to their respective drug-loaded counterpart in order to determine the sole concentration of the drug released in RPMI 1640 without background.

Cell culture

For in vitro cell biology assays, two different pancreatic cancer cell lines, namely BxPC-3 (a human pancreatic cancer cell line, CRL-1687 from ATCC) and AsPC-1 (a human pancreas adenocarcinoma ascites metastasis cell line, CRL-1682 from ATCC) were used. Cells were cultured in RPMI supplemented with 10% FBS and 1% penicillin & streptomycin antibiotic solution at 37°C and 5% CO_2 atmosphere.

Nanoconstruct uptake in cells

Flow cytometry analyses were performed to evaluate the uptake of the nanoconstruct by the pancreatic cancer cells. These experiments were executed with a flow cytometer (Guava® EasyCyte 6-“L, Merck Millipore) equipped with 647 nm laser, to track internalization of the fluorophore-labeled nanoparticles into cells. For this purpose, cells were seeded (30000 cells per well) in a 24-well plate (Greiner Bio-One) for 24h before the treatment. NCs were labeled with ATTO 647 and coated with EV-Lipo shell (with and

without target peptide), following the procedure reported in the “Extracellular vesicles and lipid coating” section. Then, the EV-Lipo and EV-Lipo-pep coated, ATTO 647 labeled NCs were administered to the cells at 30 µg/ml concentration of NCs for 20 hours. After that, cells were trypsinized and washed with PBS and subjected towards flow cytometric analysis, and the internalization rate was evaluated in terms of % of positive events, as reported in other works(56, 62).

Furthermore, for live-cell imaging optical fluorescence microscopy cells were seeded (5000 cells per well) in an 8-well chamber slide (Nunc™ Lab-Tek™ II CC2™ Chamber Slide System, Thermo Fisher Scientific™) and NCs were coated with EV-Lipo-pep shell having FITC bound to the peptide. Cell membranes were labeled with Wheat Germ Agglutinin, Alexa Fluor™ 647 Conjugate (WGA647, Thermo Fisher) and the cellular uptake of 10 µg/ml FITC-labeled nanoconstruct was assessed after 20 hours of incubation at 37°C and 5% CO_2 atmosphere.

Cytotoxicity and cellular apoptosis

The cytotoxicity of EV-Lipo-pep-NCs-Gem nanoconstruct was assessed treating both pancreatic cancer cell lines with a concentration of 30 µg of NCs/ml of RPMI complete medium for 48 hours. The nanoconstruct without Gemcitabine was used as control. Furthermore, the cells were treated with the free drug in the same amount which was loaded on the NCs. Cells were seeded (2500 cells per well) in 96-well plate (Greiner Bio-One) for 24h before the treatment. To assess cells viability after the treatment, 10 µl of WST-1 (Cell Proliferation Reagent WST-1, Roche) was added to each well and after 2 h of incubation at standard conditions, the formazan absorbance was detected at 450 nm by the Multiskan Go microplate spectrophotometer (Thermo Fisher Scientific) using a 620-nm reference.

The evaluation of apoptosis processes involved in cell death was assessed by flow cytometry, seeding 30000 cells per well in a 24-well plate for 24h before the treatment and then administering the nanoconstruct to the cells at a concentration of 30 µg/ml for 24 hours. In parallel, cells were treated with the same amount of free Gemcitabine. After the treatments, cells were trypsinized, washed with PBS, then exposed to a specific reagent (Guava® Nexin Reagent containing Annexin V and 7-AAD, Luminex) for 30 min and evaluated through flow cytometry as recommended by manufacturers.

Statistical analysis

The statistical comparison between the treatment groups was performed using one-way or two-way analysis of variance (ANOVA) with Origin software. ***$p < 0.001$ and *$p < 0.05$ were considered significant. Independent experiments were performed three-times.

Results And Discussion

Nanocrystals characterization

From the FESEM image (Fig. 2A), Gadolinium-doped NCs, synthesized with the above mentioned and previously reported(57) wet chemical co-precipitation method, show a spherical shape with a diameter

ranging from 5 to 8 nm. EDS analyses (Fig. 2B) confirm the successful inclusion of the dopant in the crystal structure, displaying a doping level of 0.37 at%.

Figure S.1 in the Supporting Information (S.I.) reports the X-Ray diffraction pattern of the NCs, showing the high crystallinity of the material in the wurtzite crystalline phase (see also Table S.1) and the absence of undesired secondary phases. More detailed characterizations, such as HRTEM and XPS were previously reported by our group(57).

To investigate the potential use of the doped nanoparticles as a contrast agent in magnetic resonance imaging, the magnetic properties of amine-functionalized Ol-ZnO-Gd NCs were measured and compared to the ones of -NH_2 functionalized but undoped Ol-ZnO NCs. Figure 2C displays the magnetic behavior of both doped and undoped NCs. While both types of NCs show paramagnetic properties, in accordance with other works(57, 63), it is worth noting that the maximum magnetization measured for an applied magnetic field of 800 kA/m strongly increases in presence of Gadolinium doping (11.8 Am^2/kg against 4.6 Am^2/kg for the undoped NCs). Since the XRD analyses of the doped NCs, in comparison to the undoped one (Fig. S.1 in the Supporting Information) confirm the absence of any undesired new crystalline phases due to the doping, the observed magnetic behavior is certainly not due to the formation, during the synthesis process, of secondary paramagnetic phases, such as Gd_2O_3(64). In contrast, the obtained results suggest that the enhanced magnetic properties of Gd-doped NCs may be a consequence of oxygen vacancies, resulting from the dopant inclusion in the crystal structure, of an exchange interaction between Gd^{3+} and Zn^{2+} ions, or of a combination between the two(65, 66). The magnetic properties measured so far can thus promote the overall nanoconstruct as an effective diagnostic tool under magnetic resonance imaging, in addition to the therapeutic capabilities which are explored below.

The DLS measurements (Fig. 2D) show a narrow hydrodynamic size distribution of the amine-functionalized, Gadolinium-doped ZnO nanocrystals, peaking at 91.3 and 106 nm (as Number %) in ethanol and water, respectively. These results, paired with the low values of the Polydispersity Index (PDI) and the relatively high value of the Zeta potential of the NCs in bidistilled water (Table 1), confirm the stability of the amine functionalized nanocrystals in the two different dispersants. It is worth to mention that the higher values resulting from the DLS measurements with respect to the size observed from the FESEM analyses can be explained by the different method of analysis, the first accounting for the hydrodynamic diameter of NCs in solution affected also by the steric hindrance of amine-functionalization and oleic capping, while the second investigating a dried sample under vacuum.

Table 1
Average hydrodynamic diameters, polydispersity index (PDI), and Zeta potential values of amine-functionalized, Gadolinium-doped ZnO nanocrystals (Ol-ZnO-Gd NCs) in ethanol and bidistilled water.

Sample	Average hydrodynamic size	PDI	Z-potential
Ol-ZnO-Gd_NCs_EtOH	91.3 nm	0.12	n.a.
Ol-ZnO-Gd_NCs _Water	106.0 nm	0.16	+ 28.8 mV

Gemcitabine Adsorption

An important step in the development of the nanoconstruct was to identify the time necessary for the drugs to be loaded on the functionalized NCs in substantial amounts. From the results of the Gemcitabine uptake optimization (Fig. 3), it is clear that the majority of the drug is adsorbed on the nanocrystals surface within the first 2 hours, and afterwards the amount of loaded Gemcitabine remains quite steady for the next four hours. In view of this data, 2 h was selected as the optimal time step for the Gemcitabine uptake for all further experiments.

Biomimetic lipid coating of NCs

The innovative EV-Lipo-pep-NCs nanoconstruct was obtained incorporating the synthesized Ol-ZnO-Gd NCs in a biomimetic shell constituted by lymphocytes-derived EVs and synthetic liposomes functionalized with a targeting peptide, as described in detail in the Material and Methods section and in Fig. 1. These experiments were conducted in absence of drug to allow the optimization of various processing parameters related to the incorporation of the Ol-ZnO-Gd NCs into the hybrid lipidic shell. To determine the size distribution of the obtained sample, NTA (Fig. 4A) and DLS measurements (Fig. 4B) were performed, both showing a narrow size distribution, indicative of a monodispersed sample. The NTA graph displays indeed a single, tight peak centered at 124 nm for the nanoconstruct, with a concentration of 5.99 x 10^9 particles/ml, while the average hydrodynamic size in %Number of the DLS is equal to 106 nm (PDI 0.288). Interestingly, the NTA distribution of EV-Lipo-pep-NCs resembles those obtained for pristine EVs and Lipo-Lipo-pep (see Fig. S.2B and S.4B of the S.I.), suggesting that the protocol implemented for creating the functional vesicle-lipid hybrid shell and incorporating the NCs does not cause important aggregation or degradation of the lipidic part.

The highly negative zeta potential value of the EV-Lipo-pep-NCs nanoconstruct (-32.1 mV, shown in Fig. 4C) justifies and further confirms the elevated stability observed by NTA and DLS measurements. More interestingly, if compared to the positive value of the naked NCs (+ 28.8 mV), it seems to suggest the complete encapsulation of the nanocrystals in the hybrid lipidic shell, since both EVs and Lipo-pep alone have a negative zeta potential value (see the Supporting Information for more details, Figures from S.2 to S.6).

To confirm this assumption, TEM analyses were performed. The resulting images (an illustrative one is depicted in Fig. 4D) display a population of NCs (the darker dots) grouped inside a round-shaped organic

shell with a diameter of around 150 nm, supporting the claim of an effective encapsulation of the NCs in the hybrid lipidic shell. More pictures are reported in Figure S.7 of the S.I.

Furthermore, the EV-Lipo-pep-NCs nanoconstruct was analyzed through fluorescence microscopy after dye labeling of each component. The microscope images (Fig. 5) show an almost perfect colocalization between the red (nanocrystals), green (liposomes), and purple (EVs) spots, with a colocalization percentage equal to 98%, indicating a great encapsulation efficacy of Ol-ZnO-Gd NCs. Moreover, the presence of both green and far-red (represented in purple) signals demonstrates the integration between EVs and functional synthetic lipid in the formation of the NCs lipid coating.

These results highlight the successful development, through the freeze-thaw technique, of a highly stable nanoconstruct with a hybrid lipidic shell, composed of EVs and peptide-conjugated liposomes, capable to effectively encapsulate the nanocrystals and bioconjugated to a targeting peptide.

Gemcitabine release in RPMI

Having successfully completed the preparation process of the whole nanoconstruct, a further important parameter to be assessed prior to cell studies is its ability to deliver drug to the desired site without releasing it before reaching the target destination. To this end, a preliminary nanoconstruct based on artificial lipids only, incorporating drug-loaded NCs, was studied. In details, the Gemcitabine-loaded Lipo-Lipo-pep-NCs nanoconstruct was compared with naked Gemcitabine-loaded ZnO-Gd NCs in terms of drug release in RPMI up to 96 hours. The results of these measurements (Fig. 6 and Figure S.8 in the S.I.) show that, while Gemcitabine is released from the naked NCs (without any burst release and with the value of drug released stabilizing after 72 hours), the lipidic coating acts as a shield in the case of the nanoconstruct, preventing the Gemcitabine release throughout the whole duration of the experiment.

These results confirm that the lipid-coated ZnO-Gd NCs can be exploited as effective nanocarriers to achieve a sustained release of Gemcitabine in in vitro conditions. The integration of cell-derived EVs in the coating shell, in addition to the target peptide, will also improve the biocompatibility of the nanoconstruct and its ability to deliver the drug to the desired site of action, establishing in principle a promising alternative to the standard treatments for pancreatic cancer.

Cellular uptake of biomimetic nanoconstruct in Pancreatic Cancer Cells

Flow cytometry analysis was performed to evaluate the internalization of the nanoconstruct, without drug, into BxPC3 and AsPC-1 cell lines (Fig. 7).

The uptake of EVs-liposomes coated nanoconstruct with and without target peptide is reported for both cell lines in Fig. 7. It becomes evident that the presence of the peptide leads to a significant increase of ~ 20% of positive events into both cell lines with respect to the same nanoconstruct without the peptide. The total amount of positive cells uptaking the EV-Lipo-pep-NCs nanoconstruct is very high, largely over 85%, for both the cell line.

The internalization of EV-Lipo-pep-NCs was also qualitatively evaluated through fluorescence microscopy under live-cell imaging in BxPC-3 (Fig. 8A) and AsPC-1 (Fig. 8B) cell lines. The results are in accordance with cytofluorimetric analysis, showing that, especially for BxPC3, almost all the green spots (related to the NCs shell) are inside the cellular membrane (in purple), indicating a complete internalization of the nanoconstruct inside the target cells. Control experiments on untreated cells imaged in the same channels are reported in Figure S.9 of the S.I., evidencing the absence any green background.

Therapeutic enhanced activity by gemcitabine biomimetic nanoconstruct

Following the above optimizations, Gemcitabine was loaded on the Ol-ZnO-Gd NCs surface and then EVs and lipid coating was performed (as reported in the Materials and Methods section). The final nanoconstruct (EV-Lipo-pep-NCs-Gem) was tested to evaluate its therapeutic effects on human pancreatic cell line (BxPC3), and its human metastatic counterpart (AsPC-1), after 48 hours of incubation (Fig. 9). The two pancreatic tumor cell lines were treated with 30 μg/ml of doped NCs encapsulated in the hybrid lipidic shell, with and without the drug loaded on NCs surface. This concentration value was selected based on the results of preliminary tests performed with the Lipo-Lipo-pep-NCs nanoconstruct, as reported in Figure S.10 of the S.I.

With the aim of comparing the efficacy of the nanoconstruct with the free drug, cells were also treated with Gemcitabine alone, in the same amount loaded on the NCs counterpart.

When BxPC-3 and AsPC-1 were treated with the pristine EV-Lipo-pep-NCs (without drug), cell viability remains elevated, widely over the 80% with respect to the untreated cells, underlining that the nanoconstruct itself is safe and biocompatible at the selected dosage. On the other side, when Gemcitabine is loaded and delivered through the nanoconstruct, the cytotoxic effect increases for both the cell lines. In particular, the drug-loaded nanoconstruct displays a higher efficacy compared to the free drug itself, decreasing the cell viability from 60% for Gemcitabine alone to 30–40% for EV-Lipo-pep-NCs-Gem. Even if the standard deviation is slightly larger, the drug-loaded nanoconstruct causes a higher decrease in cell metabolic activity for BxPC-3 with respect to the metastatic cell line.

Despite its efficacy, the cell killing mechanism remains unclear and to further investigate this aspect, apoptosis assays were performed on both BxPC3 and AsPC-1 cell lines. Gemcitabine-loaded nanoconstruct were incubated at the concentration of 30 μg/ml for 24h in both cell culture and the effect are compared with untreated cells or cells treated with free Gemcitabine, at the same concentration of the drug encapsulated in the nanoconstruct (Fig. 10).

The apoptosis assay is based on the fluorescence emission analyzed with flow cytometry. During the apoptotic process, cells expose molecules of PS on the external side of their membrane, which binds to Annexin V conjugated to the fluorescent dye PE, labeling these specific cells as apoptotic ones. The other dye, 7-AAD, is a fluorescent intercalator of DNA, that can be bound to cells genetic material only if cell membranes integrity is perturbed, as in case of necrosis or late apoptosis. Therefore, three populations

are identified: viable cells (negative for both AnnexinV-PE and 7-AAD), early-apoptotic cells (positive for AnnexinV-PE and negative for 7-AAD) and necrotic or late stage of apoptosis cells (positive for both AnnexinV-PE and 7-AAD)(67).

The population of untreated cells is evaluated as a control (Fig. 10, left side panels in A and B). For BxPC-3 cells, the therapeutic effect of the drug-loaded nanoconstruct proves to be extremely higher with respect to Gemcitabine alone (40.47% of dead cells compared to 12.21%, and 9.76% of early apoptotic cells when treated with the nanoconstruct with respect to 9.31% using the free drug). AsPC-1 cell line showed a similar behavior but in this case the efficacy of the drug-loaded nanoconstruct is just slightly superior compared to the free drug (5.33% of dead cells with respect to 3.50%, and for early apoptotic cells 7.28% with nanoconstruct versus 5.26% with free drug). These results underline the extraordinary potential of this nanoconstruct for pancreatic cancer treatment, while also showing its greater effectiveness towards cancer cells (BxPC-3) compared to the metastatic ones (AsPC-1). Furthermore, the plots confirm that the nanoconstruct used as a drug delivery system improves Gemcitabine efficacy without altering its mechanism of action, which leads cells to apoptosis(59, 68).

Conclusions

This work reports on the optimization process that leads to obtain an innovative theranostic nanoconstruct, where for the first time Gemcitabine was loaded on Gd-doped nanocrystals coated with a hybrid lipidic shell composed of extracellular vesicles and liposomes linked to a specific target peptide. This study goes beyond the optimization and characterization steps, testing the nanoconstruct in vitro on two different pancreatic cell lines.

The synthesis of Gd-doped ZnO NCs, here reported, was performed through a wet chemical co-precipitation method, obtaining reproducible and stable batches of NCs, which can be stored in both ethanol and water. The NCs were then functionalized with amino-propyl groups on the surface: FESEM, DLS, Z-potential, and X-ray diffraction analyses confirm the successful synthesis and the effectiveness of the functionalization. Furthermore, to explore the possibility of exploiting the nanoconstruct not only as a therapeutic agent but also as a diagnostic one, the magnetic properties of the Gd-doped NCs were measured and compared to the pristine ZnO NCs' ones, confirming the multifunctional potential of this innovative nanoconstruct.

Moving towards the creation of a theranostic tool, Gemcitabine was loaded on the functionalized, Gd-doped ZnO NCs. A further step was made, coating the NCs with an innovative hybrid lipidic shell, through a freeze-thaw process and characterizing the obtained nanoconstruct (EV-Lipo-pep-NCs) in terms of NTA, DLS, Z-potential, TEM, and fluorescence microscopy.

Special attention was given to the bioconjugation of the targeting agent, the CKAAKN synthetic peptide, which was successfully linked to DSPE-PEG(2000)Maleimide lipids and added to the already formed DOPC liposomes.

These optimal results led to the in vitro testing of the nanoconstruct into two different pancreatic cancer cell lines: a human pancreatic cell line (BxPC3), and its human metastatic counterpart (AsPC-1). Remarkable results were then obtained. Considering an optimized concentration equal to 30 μg/ml, EV-Lipo-pep-NCs was not cytotoxic for both the cell lines, and the equivalent amount of drug loaded on the NCs is not particularly toxic for both cell lines when administered as a free drug, but when this dose is loaded on the NCs surface, the cytotoxic effect of the EV-Lipo-pep-NCs-Gem nanoconstruct becomes evident in both cell lines, confirming the efficacy of the generated nanotool. Therefore, the theranostic approach is more appealing not only for the multiple actions of the nanoconstruct (therapy and diagnosis), but also for the larger effectiveness with respect to the conventional treatments used in clinics. Furthermore, cellular uptake is actually increased with the presence of the targeting peptide, reaching an internalization of the final nanoconstruct close to 90%. These results were also confirmed by fluorescence images, showing their presence inside the cellular membrane for both the cell lines.

The last investigation was related to the study of the killing mechanism of the nanosconstruct, showing that the presence of the drug-loaded nanoconstruct strongly enhances the Gemcitabine therapeutic efficacy without altering its mechanism of action.

These results highlight the efficacy of the innovative theranostic nanocarrier loaded with Gemcitabine, which can prove to be a valid alternative to the standard approaches to treat pancreatic cancer.

Declarations

ASSOCIATED CONTENT

Supporting Information. The following files are available free of charge:
Doped and undoped NCs characterizations; Extracellular vesicles characterizations; Liposomes coating; Lipo-Lipo-pep-NCs nanoconstruct characterizations; Additional TEM images of the optimized EV-Lipo-pep-NCs nanoconstruct; Drug delivery expressed in percentage; Cellular uptake of biomimetic nanoconstruct in Pancreatic Cancer Cells: control experiments; Preliminary tests on cytotoxicity of the Lipo-Lipo-pep-NCs-Gem.

AUTHOR INFORMATION

Corresponding Author

* Prof Valentina Cauda, Department of Applied Science and Technology, Politecnico di Torino, Turin, Italy; e-mail: valetina.cauda@polito.it ; phone: +39 011 0907389

AUTHORS' CONTRIBUTIONS

S.B. and V.C. conceptualize the project idea and received funding. N.M.P. wrote the main manuscript text and prepared Figures 1-6 and the Supporting Information. S.B. performed cell investigations and prepared Figures 7-10. S.B., N.M.P, M.C., B.D. L.R. M.C. developed the adopted methodology. S.B., N.M.P, M.C.

performed the experimental investigation. V.C. supervised the team, managed the project and related funding. All authors reviewed the manuscript and contributed to the scientific discussion. All authors have given approval to the final version of the manuscript. ‡These authors contributed equally.

ETHICS APPROVAL AND CONSENT TO PARTICIPATE

Not applicable.

CONSENT FOR PUBLICATION

All authors have given their consent to publication

AVAILABILITY OF DATA AND MATERIALS

All data generated or analysed during this study are included in this published article and its supplementary information files.

COMPETING INTEREST

The authors declare that they have no competing interests.

FUNDING

This work has received funding from the European Commission under a Marie Skłodowska–Curie Actions grant (Standard European Individual Fellowships, H2020-MSCA-IF-2018, Grant Agreement No. 842964, Project Acronym “MINT”).

ACKNOWLEDGMENTS

Dr. Marco Allione is gratefully acknowledged for the acquisition of TEM images.

References

1. Key Statistics for Pancreatic Cancer [Internet]. [cited 2022 May 10]. Available from: https://www.cancer.org/cancer/pancreatic-cancer/about/key-statistics.html
2. Zhang L, Sanagapalli S, Stoita A. Challenges in diagnosis of pancreatic cancer. World Journal of Gastroenterology. 2018 May 21;24(19):2047–60.
3. Bailey P, Chang DK, Nones K, Johns AL, Patch AM, Gingras MC, et al. Genomic analyses identify molecular subtypes of pancreatic cancer. Nature. 2016 Mar;531(7592):47–52.
4. Polireddy K, Chen Q. Cancer of the Pancreas: Molecular Pathways and Current Advancement in Treatment. J Cancer. 2016;7(11):1497–514.
5. Puri S, Folias AE, Hebrok M. Plasticity and dedifferentiation within the pancreas: development, homeostasis, and disease. Cell Stem Cell. 2015 Jan 8;16(1):18–31.

6. Cannon A, Thompson C, Hall BR, Jain M, Kumar S, Batra SK. Desmoplasia in pancreatic ductal adenocarcinoma: insight into pathological function and therapeutic potential. Genes Cancer. 2018 Mar;9(3–4):78–86.
7. Erkan M, Kurtoglu M, Kleeff J. The role of hypoxia in pancreatic cancer: a potential therapeutic target? Expert Rev Gastroenterol Hepatol. 2016;10(3):301–16.
8. Looi CK, Chung FFL, Leong CO, Wong SF, Rosli R, Mai CW. Therapeutic challenges and current immunomodulatory strategies in targeting the immunosuppressive pancreatic tumor microenvironment. Journal of Experimental & Clinical Cancer Research. 2019 Apr 15;38(1):162.
9. Cannistrà M, Ruggiero M, Zullo A, Serafini S, Grande R, Nardo B. Metastases of pancreatic adenocarcinoma: A systematic review of literature and a new functional concept. International Journal of Surgery. 2015 Sep 1;21:S15–21.
10. Yu S, Zhang C, Xie KP. Therapeutic resistance of pancreatic cancer: Roadmap to its reversal. Biochimica et Biophysica Acta (BBA) - Reviews on Cancer. 2021 Jan 1;1875(1):188461.
11. Zhou B, Xu JW, Cheng YG, Gao JY, Hu SY, Wang L, et al. Early detection of pancreatic cancer: Where are we now and where are we going? Int J Cancer. 2017 Jul 15;141(2):231–41.
12. Bengtsson A, Andersson R, Ansari D. The actual 5-year survivors of pancreatic ductal adenocarcinoma based on real-world data. Sci Rep. 2020 Oct 2;10(1):16425.
13. Oettle H, Neuhaus P, Hochhaus A, Hartmann JT, Gellert K, Ridwelski K, et al. Adjuvant Chemotherapy With Gemcitabine and Long-term Outcomes Among Patients With Resected Pancreatic Cancer: The CONKO-001 Randomized Trial. JAMA. 2013 Oct 9;310(14):1473–81.
14. O'Reilly EM, Ferrone C. Neoadjuvant or Adjuvant Therapy for Resectable or Borderline Resectable Pancreatic Cancer: Which Is Preferred? J Clin Oncol. 2020 Jun 1;38(16):1757–9.
15. Mokdad AA, Minter RM, Zhu H, Augustine MM, Porembka MR, Wang SC, et al. Neoadjuvant Therapy Followed by Resection Versus Upfront Resection for Resectable Pancreatic Cancer: A Propensity Score Matched Analysis. JCO. 2017 Feb 10;35(5):515–22.
16. Chin V, Nagrial A, Sjoquist K, O'Connor CA, Chantrill L, Biankin AV, et al. Chemotherapy and radiotherapy for advanced pancreatic cancer. Cochrane Database Syst Rev. 2018 Mar 20;3:CD011044.
17. Wang WB, Yang Y, Zhao YP, Zhang TP, Liao Q, Shu H. Recent studies of 5-fluorouracil resistance in pancreatic cancer. World Journal of Gastroenterology. 2014 Nov 14;20(42):15682–90.
18. Burris HA, Moore MJ, Andersen J, Green MR, Rothenberg ML, Modiano MR, et al. Improvements in survival and clinical benefit with gemcitabine as first-line therapy for patients with advanced pancreas cancer: a randomized trial. J Clin Oncol. 1997 Jun;15(6):2403–13.
19. Poplin E, Wasan H, Rolfe L, Raponi M, Ikdahl T, Bondarenko I, et al. Randomized, Multicenter, Phase II Study of CO-101 Versus Gemcitabine in Patients With Metastatic Pancreatic Ductal Adenocarcinoma: Including a Prospective Evaluation of the Role of hENT1 in Gemcitabine or CO-101 Sensitivity. JCO. 2013 Dec 10;31(35):4453–61.

20. Bernhard J, Dietrich D, Scheithauer W, Gerber D, Bodoky G, Ruhstaller T, et al. Clinical Benefit and Quality of Life in Patients With Advanced Pancreatic Cancer Receiving Gemcitabine Plus Capecitabine Versus Gemcitabine Alone: A Randomized Multicenter Phase III Clinical Trial—SAKK 44/00–CECOG/PAN.1.3.001. JCO. 2008 Aug;26(22):3695–701.
21. Heinemann V, Quietzsch D, Gieseler F, Gonnermann M, Schönekäs H, Rost A, et al. Randomized Phase III Trial of Gemcitabine Plus Cisplatin Compared With Gemcitabine Alone in Advanced Pancreatic Cancer. JCO. 2006 Aug 20;24(24):3946–52.
22. Louvet C, Labianca R, Hammel P, Lledo G, Zampino MG, André T, et al. Gemcitabine in combination with oxaliplatin compared with gemcitabine alone in locally advanced or metastatic pancreatic cancer: results of a GERCOR and GISCAD phase III trial. J Clin Oncol. 2005 May 20;23(15):3509–16.
23. Poplin E, Feng Y, Berlin J, Rothenberg ML, Hochster H, Mitchell E, et al. Phase III, Randomized Study of Gemcitabine and Oxaliplatin Versus Gemcitabine (fixed-dose rate infusion) Compared With Gemcitabine (30-minute infusion) in Patients With Pancreatic Carcinoma E6201: A Trial of the Eastern Cooperative Oncology Group. JCO. 2009 Aug 10;27(23):3778–85.
24. Suker M, Beumer BR, Sadot E, Marthey L, Faris JE, Mellon EA, et al. FOLFIRINOX for locally advanced pancreatic cancer: a systematic review and patient-level meta-analysis. Lancet Oncol. 2016 Jun;17(6):801–10.
25. Conroy T, Desseigne F, Ychou M, Bouché O, Guimbaud R, Bécouarn Y, et al. FOLFIRINOX versus Gemcitabine for Metastatic Pancreatic Cancer. New England Journal of Medicine. 2011 May 12;364(19):1817–25.
26. Narayanan V, Weekes CD. Nanoparticle albumin-bound (nab)-paclitaxel for the treatment of pancreas ductal adenocarcinoma. GICTT. 2015 Jan 6;5:11–9.
27. Belalcazar A, Nagaraju GP. Chapter 3 - Current knowledge on drug resistance and therapeutic approaches to eliminate pancreatic cancer stem cells. In: Nagaraju GP, Ahmad S, editors. Theranostic Approach for Pancreatic Cancer [Internet]. Academic Press; 2019 [cited 2022 May 10]. p. 69–80. Available from: https://www.sciencedirect.com/science/article/pii/B9780128194577000037
28. Adamska A, Elaskalani O, Emmanouilidi A, Kim M, Abdol Razak NB, Metharom P, et al. Molecular and cellular mechanisms of chemoresistance in pancreatic cancer. Adv Biol Regul. 2018 May;68:77–87.
29. Pàez-Ribes M, Allen E, Hudock J, Takeda T, Okuyama H, Viñals F, et al. Antiangiogenic therapy elicits malignant progression of tumors to increased local invasion and distant metastasis. Cancer Cell. 2009 Mar 3;15(3):220–31.
30. Adamska A, Domenichini A, Falasca M. Pancreatic Ductal Adenocarcinoma: Current and Evolving Therapies. Int J Mol Sci. 2017 Jun 22;18(7):E1338.
31. Kota J, Hancock J, Kwon J, Korc M. Pancreatic cancer: Stroma and its current and emerging targeted therapies. Cancer Letters. 2017 Apr 10;391:38–49.
32. Hansem LMK, Huang R, Wegner CS, Simonsen TG, Gaustad JV, Hauge A, et al. Intratumor Heterogeneity in Interstitial Fluid Pressure in Cervical and Pancreatic Carcinoma Xenografts. Translational Oncology. 2019 Aug 1;12(8):1079–85.

33. Annese T, Tamma R, Ruggieri S, Ribatti D. Angiogenesis in Pancreatic Cancer: Pre-Clinical and Clinical Studies. Cancers. 2019 Mar;11(3):381.
34. Neesse A, Krug S, Gress TM, Tuveson DA, Michl P. Emerging concepts in pancreatic cancer medicine: targeting the tumor stroma. OTT. 2013 Dec 18;7:33–43.
35. Greene MK, Johnston MC, Scott CJ. Nanomedicine in Pancreatic Cancer: Current Status and Future Opportunities for Overcoming Therapy Resistance. Cancers (Basel). 2021 Dec 7;13(24):6175.
36. Ortíz R, Quiñonero F, García-Pinel B, Fuel M, Mesas C, Cabeza L, et al. Nanomedicine to Overcome Multidrug Resistance Mechanisms in Colon and Pancreatic Cancer: Recent Progress. Cancers. 2021 Jan;13(9):2058.
37. Shi J, Kantoff PW, Wooster R, Farokhzad OC. Cancer nanomedicine: progress, challenges and opportunities. Nat Rev Cancer. 2017 Jan;17(1):20–37.
38. Kim MP, Gallick GE. Gemcitabine resistance in pancreatic cancer: picking the key players. Clin Cancer Res. 2008 Mar 1;14(5):1284–5.
39. Binenbaum Y, Na'ara S, Gil Z. Gemcitabine resistance in pancreatic ductal adenocarcinoma. Drug Resistance Updates. 2015 Nov 1;23:55–68.
40. Weizman N, Krelin Y, Shabtay-Orbach A, Amit M, Binenbaum Y, Wong RJ, et al. Macrophages mediate gemcitabine resistance of pancreatic adenocarcinoma by upregulating cytidine deaminase. Oncogene. 2014 Jul 17;33(29):3812–9.
41. Samanta K, Setua S, Kumari S, Jaggi M, Yallapu MM, Chauhan SC. Gemcitabine Combination Nano Therapies for Pancreatic Cancer. Pharmaceutics. 2019 Nov;11(11):574.
42. Dadwal A, Baldi A, Kumar Narang R. Nanoparticles as carriers for drug delivery in cancer. Artificial Cells, Nanomedicine, and Biotechnology. 2018 Nov 5;46(sup2):295–305.
43. Yao Y, Zhou Y, Liu L, Xu Y, Chen Q, Wang Y, et al. Nanoparticle-Based Drug Delivery in Cancer Therapy and Its Role in Overcoming Drug Resistance. Frontiers in Molecular Biosciences [Internet]. 2020 [cited 2022 May 10];7. Available from: https://www.frontiersin.org/article/10.3389/fmolb.2020.00193
44. Estelrich J, Sánchez-Martín MJ, Busquets MA. Nanoparticles in magnetic resonance imaging: from simple to dual contrast agents. Int J Nanomedicine. 2015 Mar 6;10:1727–41.
45. Carofiglio M, Barui S, Cauda V, Laurenti M. Doped Zinc Oxide Nanoparticles: Synthesis, Characterization and Potential Use in Nanomedicine. Applied Sciences. 2020 Jul 28;10(15):5194.
46. Luchini A, Vitiello G. Understanding the Nano-bio Interfaces: Lipid-Coatings for Inorganic Nanoparticles as Promising Strategy for Biomedical Applications. Frontiers in Chemistry [Internet]. 2019 [cited 2022 May 10];7. Available from: https://www.frontiersin.org/article/10.3389/fchem.2019.00343
47. Carofiglio M, Laurenti M, Genchi GG, Ciofani G, Grochowicz M, Cauda V. Ultrasound Triggered ZnO-Based Devices for Tunable and Multifaceted Biomedical Applications. Advanced Materials Interfaces. 2021;8(21):2101021.

48. Racca L, Canta M, Dumontel B, Ancona A, Limongi T, Garino N, et al. Zinc Oxide Nanostructures in Biomedicine. In: Smart Nanoparticles for Biomedicine [Internet]. Elsevier; 2018 [cited 2019 Jun 7]. p. 171–87. Available from: https://linkinghub.elsevier.com/retrieve/pii/B9780128141564000124
49. Dumontel B, Canta M, Engelke H, Chiodoni A, Racca L, Ancona A, et al. Enhanced biostability and cellular uptake of zinc oxide nanocrystals shielded with a phospholipid bilayer. J Mater Chem B. 2017 Nov 15;5(44):8799–813.
50. Ancona A, Dumontel B, Garino N, Demarco B, Chatzitheodoridou D, Fazzini W, et al. Lipid-Coated Zinc Oxide Nanoparticles as Innovative ROS-Generators for Photodynamic Therapy in Cancer Cells. Nanomaterials. 2018 Mar 2;8(3):143.
51. Zeng K, Li J, Zhang Z, Yan M, Liao Y, Zhang X, et al. Lipid-coated ZnO nanoparticles as lymphatic-targeted drug carriers: study on cell-specific toxicity in vitro and lymphatic targeting in vivo. J Mater Chem B. 2015 Jun 25;3(26):5249–60.
52. Srivastava A, Amreddy N, Babu A, Panneerselvam J, Mehta M, Muralidharan R, et al. Nanosomes carrying doxorubicin exhibit potent anticancer activity against human lung cancer cells. Sci Rep. 2016 Dec 12;6(1):38541.
53. Susa F, Limongi T, Dumontel B, Vighetto V, Cauda V. Engineered Extracellular Vesicles as a Reliable Tool in Cancer Nanomedicine. Cancers. 2019 Dec;11(12):1979.
54. Patil SM, Sawant SS, Kunda NK. Exosomes as drug delivery systems: A brief overview and progress update. Eur J Pharm Biopharm. 2020 Sep;154:259–69.
55. Dumontel B, Susa F, Limongi T, Canta M, Racca L, Chiodoni A, et al. ZnO nanocrystals shuttled by extracellular vesicles as effective Trojan nano-horses against cancer cells. Nanomedicine. 2019 Nov;14(21):2815–33.
56. Dumontel B, Susa F, Limongi T, Vighetto V, Debellis D, Canta M, et al. Nanotechnological engineering of extracellular vesicles for the development of actively targeted hybrid nanodevices. Cell & Bioscience. 2022 May 14;12(1):61.
57. Barui S, Gerbaldo R, Garino N, Brescia R, Laviano F, Cauda V. Facile Chemical Synthesis of Doped ZnO Nanocrystals Exploiting Oleic Acid. Nanomaterials (Basel). 2020 Jun 11;10(6):1150.
58. Valetti S, Maione F, Mura S, Stella B, Desmaële D, Noiray M, et al. Peptide-functionalized nanoparticles for selective targeting of pancreatic tumor. J Control Release. 2014 Oct 28;192:29–39.
59. Pardo R, Ré AL, Archange C, Ropolo A, Papademetrio DL, Gonzalez CD, et al. Gemcitabine Induces the VMP1-Mediated Autophagy Pathway to Promote Apoptotic Death in Human Pancreatic Cancer Cells. PAN. 2010;10(1):19–26.
60. Cauda V, Engelke H, Sauer A, Arcizet D, Christoph Bräuchle, Rädler J, et al. Colchicine-Loaded Lipid Bilayer-Coated 50 nm Mesoporous Nanoparticles Efficiently Induce Microtubule Depolymerization upon Cell Uptake. Nano Lett. 2010 Jul 14;10(7):2484–92.
61. Limongi T, Susa F, Dumontel B, Racca L, Perrone Donnorso M, Debellis D, et al. Extracellular Vesicles Tropism: A Comparative Study between Passive Innate Tropism and the Active Engineered Targeting Capability of Lymphocyte-Derived EVs. Membranes. 2021 Nov;11(11):886.

62. Vighetto V, Racca L, Canta M, Matos JC, Dumontel B, Gonçalves MC, et al. Smart Shockwave Responsive Titania-Based Nanoparticles for Cancer Treatment. Pharmaceutics. 2021 Sep 8;13(9):1423.
63. Carofiglio M, Laurenti M, Vighetto V, Racca L, Barui S, Garino N, et al. Iron-Doped ZnO Nanoparticles as Multifunctional Nanoplatforms for Theranostics. Nanomaterials. 2021 Oct 6;11(10):2628.
64. Moon RM, Koehler WC. Magnetic properties of Gd 2 O 3. Phys Rev B. 1975 Feb 15;11(4):1609–22.
65. Poornaprakash B, Chalapathi U, Babu S, Park SH. Structural, morphological, optical, and magnetic properties of Gd-doped and (Gd, Mn) co-doped ZnO nanoparticles. Physica E: Low-dimensional Systems and Nanostructures. 2017 Sep;93:111–5.
66. Vijayaprasath G, Murugan R, Hayakawa Y, Ravi G. Optical and magnetic studies on Gd doped ZnO nanoparticles synthesized by co-precipitation method. Journal of Luminescence. 2016 Oct;178:375–83.
67. Guava® Nexin Reagent [Internet]. Luminex Corporation. [cited 2021 Nov 23]. Available from: https://www.luminexcorp.com/guava-nexin-reagent/
68. Huang P, Plunkett W. Induction of apoptosis by gemcitabine. Semin Oncol. 1995 Aug 1;22(4 Suppl 11):19–25.

Supporting Information

Supporting Information Figure S1 is not available with this version

Figures

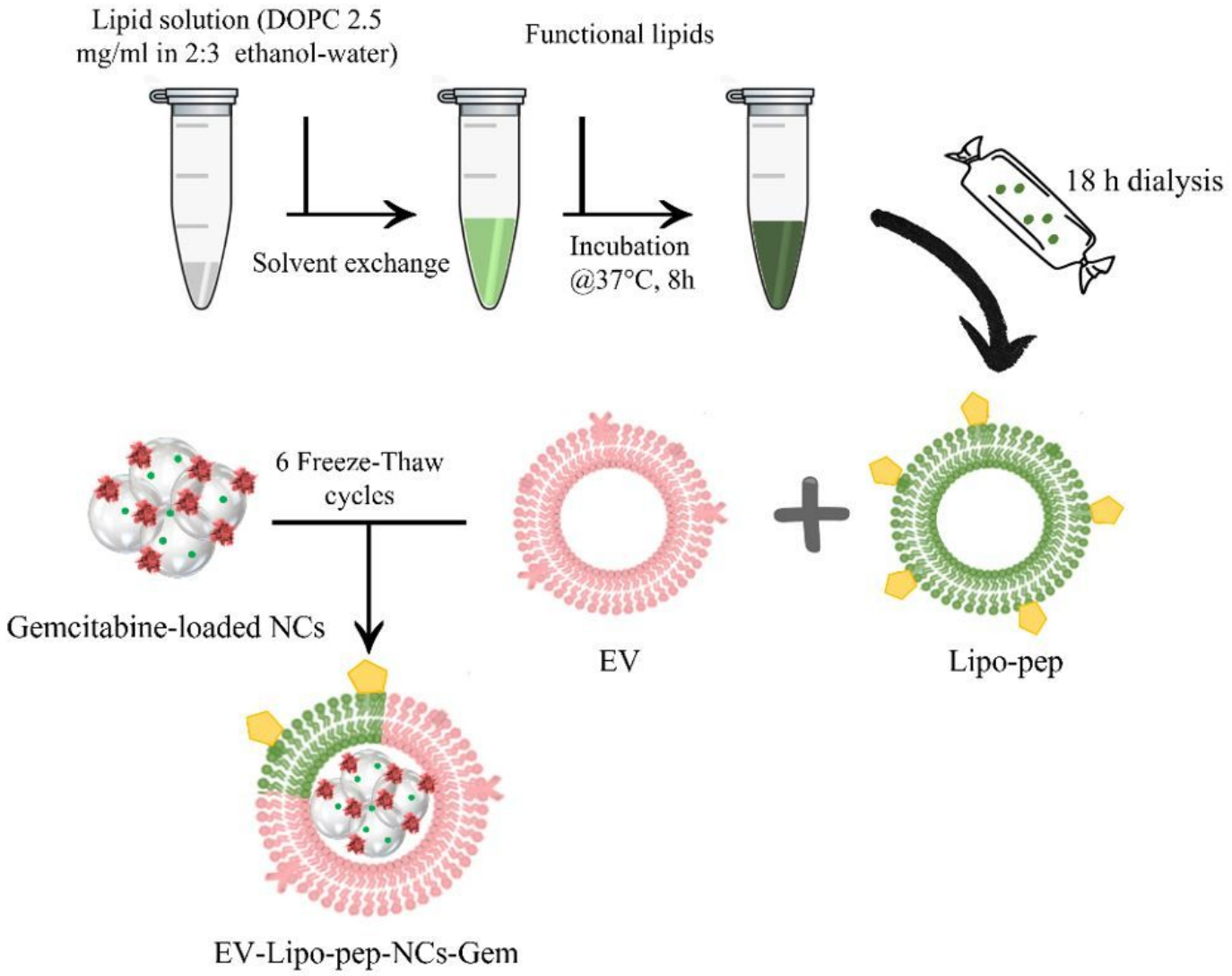

Figure 1

Scheme of extracellular vesicles (EV) and DOPC:DSPE-PEG-CKAAKN liposomes (Lipo-pep) coating on Gemcitabine-loaded ZnO-Gd NCs through freeze-thaw process.

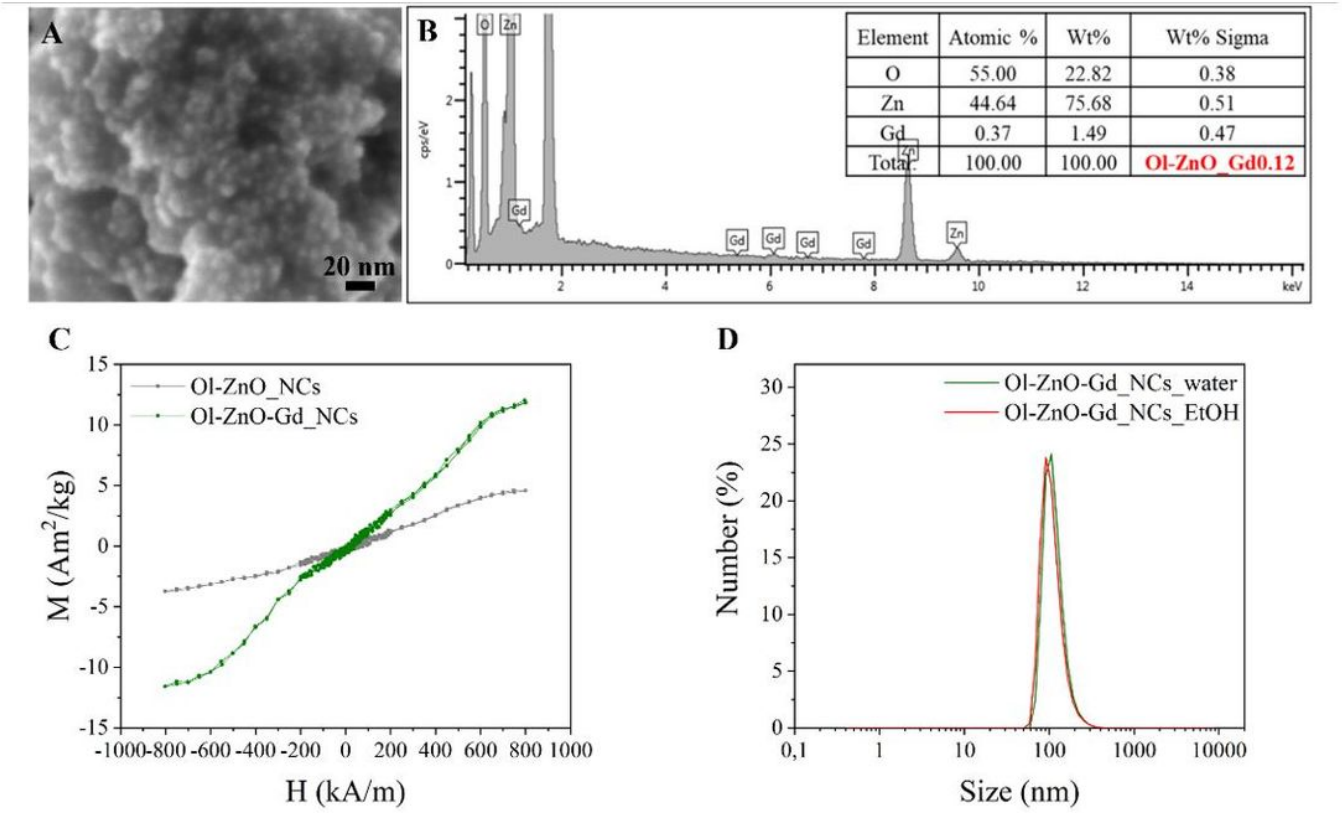

Figure 2

Characterization of the Gadolinium-doped Ol-ZnO NCs: (A) Field emission scanning electron microscopy (FESEM) image and (B) Energy dispersive X-ray spectroscopy (EDS) confirming the successful inclusion of the dopant on the NCs prior to amino-functionalization (only O, Zn, and Gd were considered in the analysis). (C) Magnetization–saturation (M-H) curves comparing the magnetic behavior of amine-functionalized Ol-ZnO (gray curve) and Ol-ZnO-Gd (green curve) NCs. (D) Size distribution resulting from Dynamic Light Scattering (DLS) measurements of amine-functionalized Ol-ZnO-Gd nanocrystals in ethanol (red line) and water (green line).

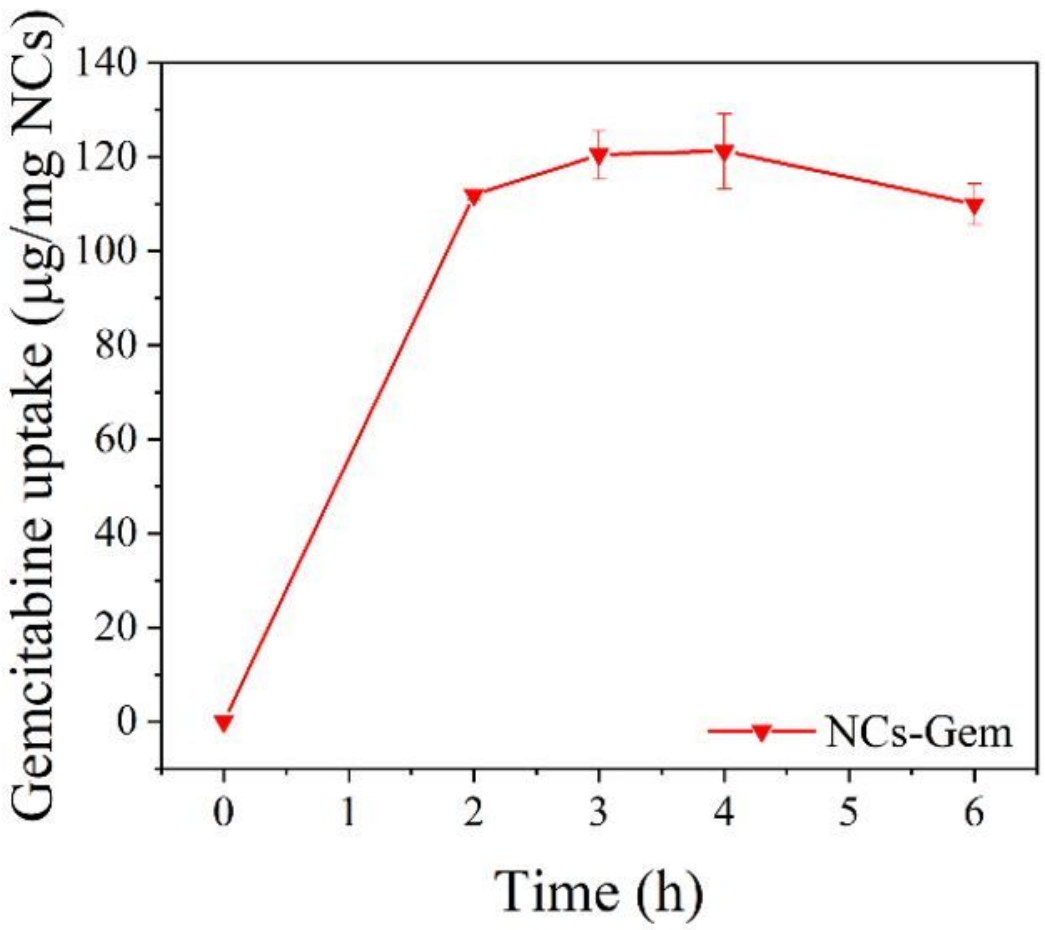

Figure 3

Gemcitabine uptake optimization in bidistilled water on amine-functionalized, Gd-doped Ol-ZnO NCs (here NCs-Gem), expressed in µg of drug per mg of nanocrystals.

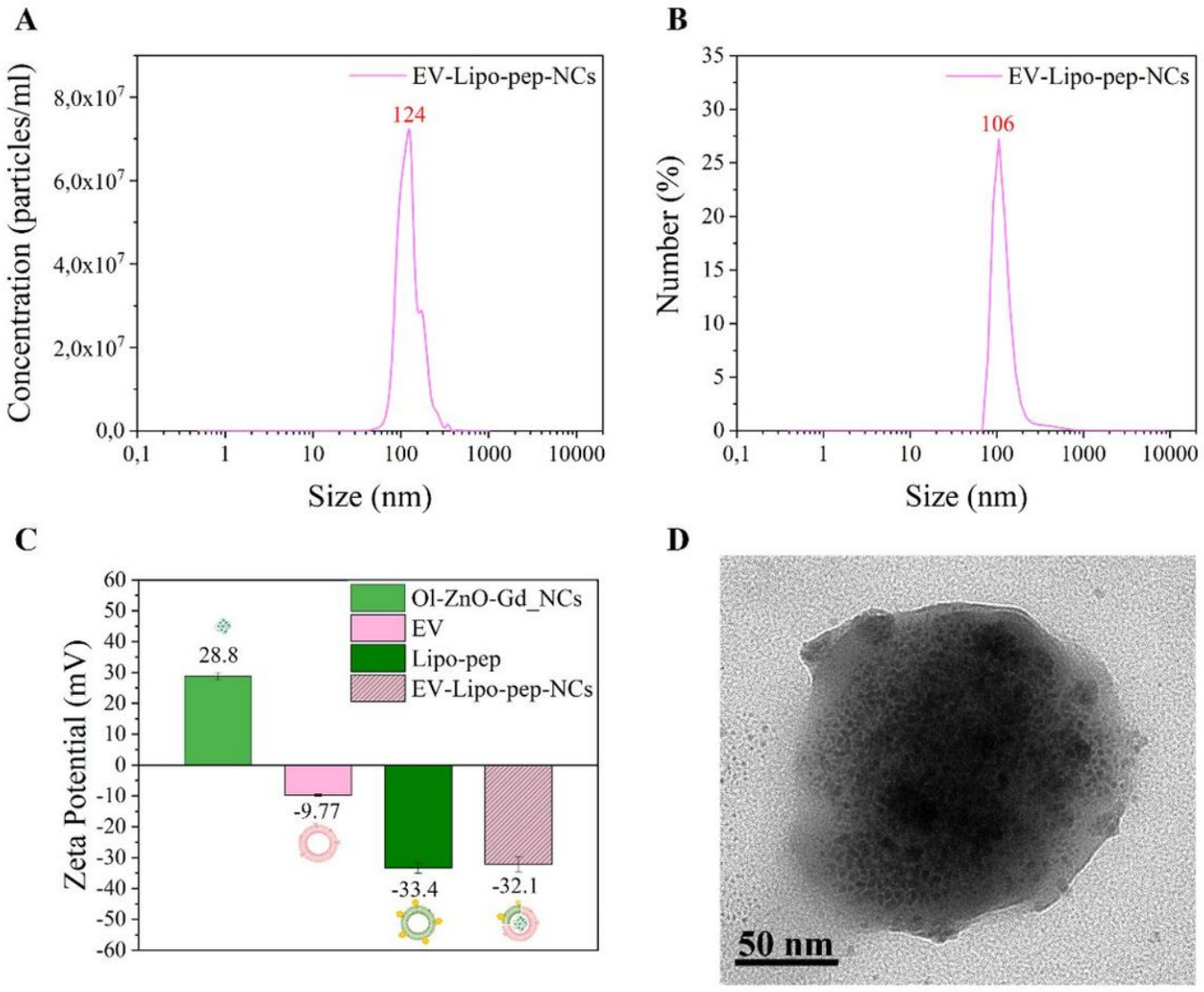

Figure 4

Characterization of EV-Lipo-pep-NCs: size distribution resulting from (A) NTA and (B) DLS measurements of the EV-Lipo-pep-NCs nanoconstruct. (C) Comparison between zeta potential values of uncoated NCs, EVs, Lipo-pep, and EV-Lipo-pep coated NCs. (D) TEM image at 60 kV of the nanoconstruct.

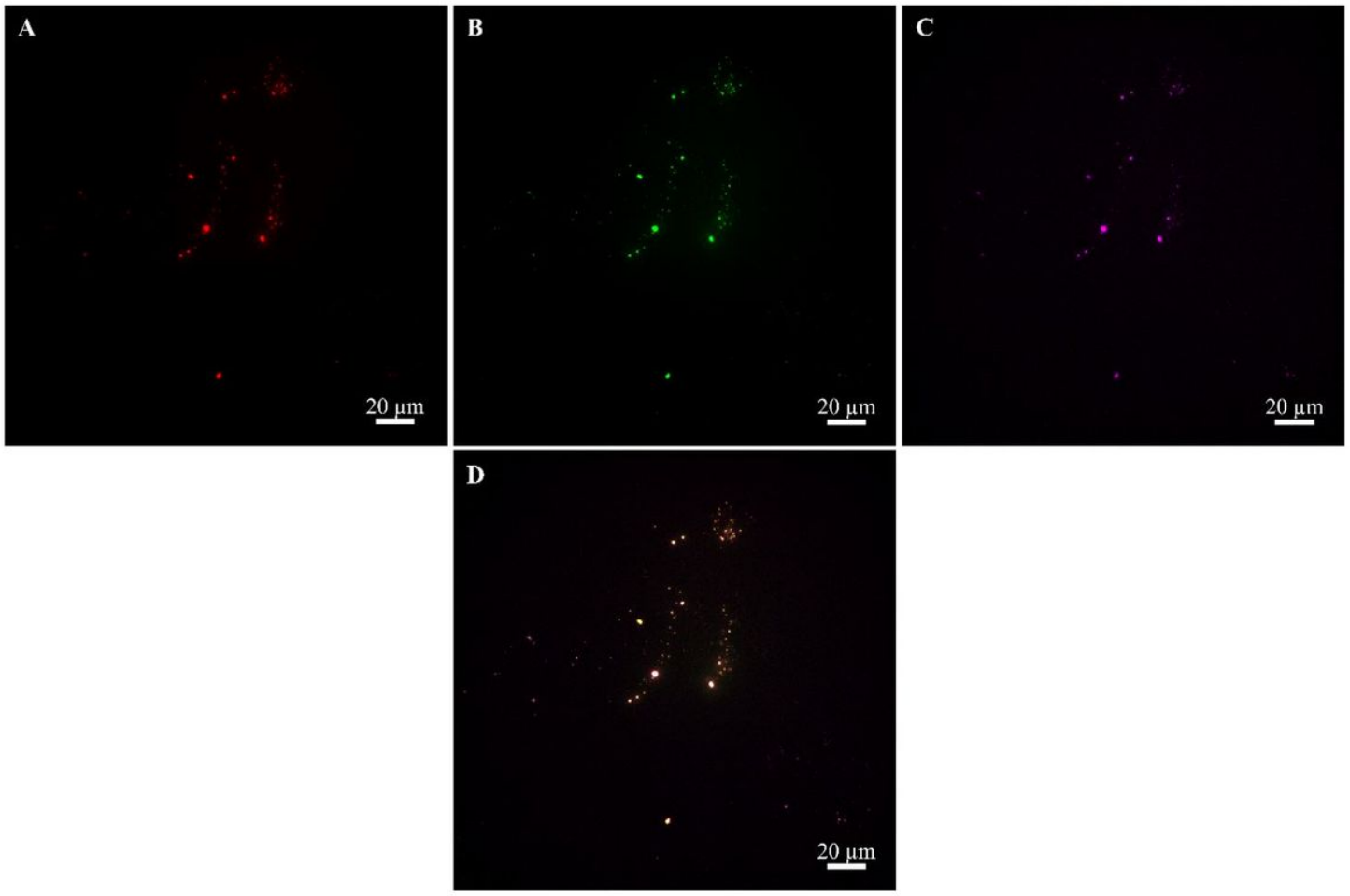

Figure 5

Fluorescence microscope images of the dyes labeled EV-Lipo-pep-NCs nanoconstruct: (A) Red channel showing Atto550 bound to NCs, (B) green channel highlighting FITC bound to the peptide, (C) far-red channel (represented in purple) displaying WGA647 bound to the EVs and (D) merged images. Scale bars: 20 µm.

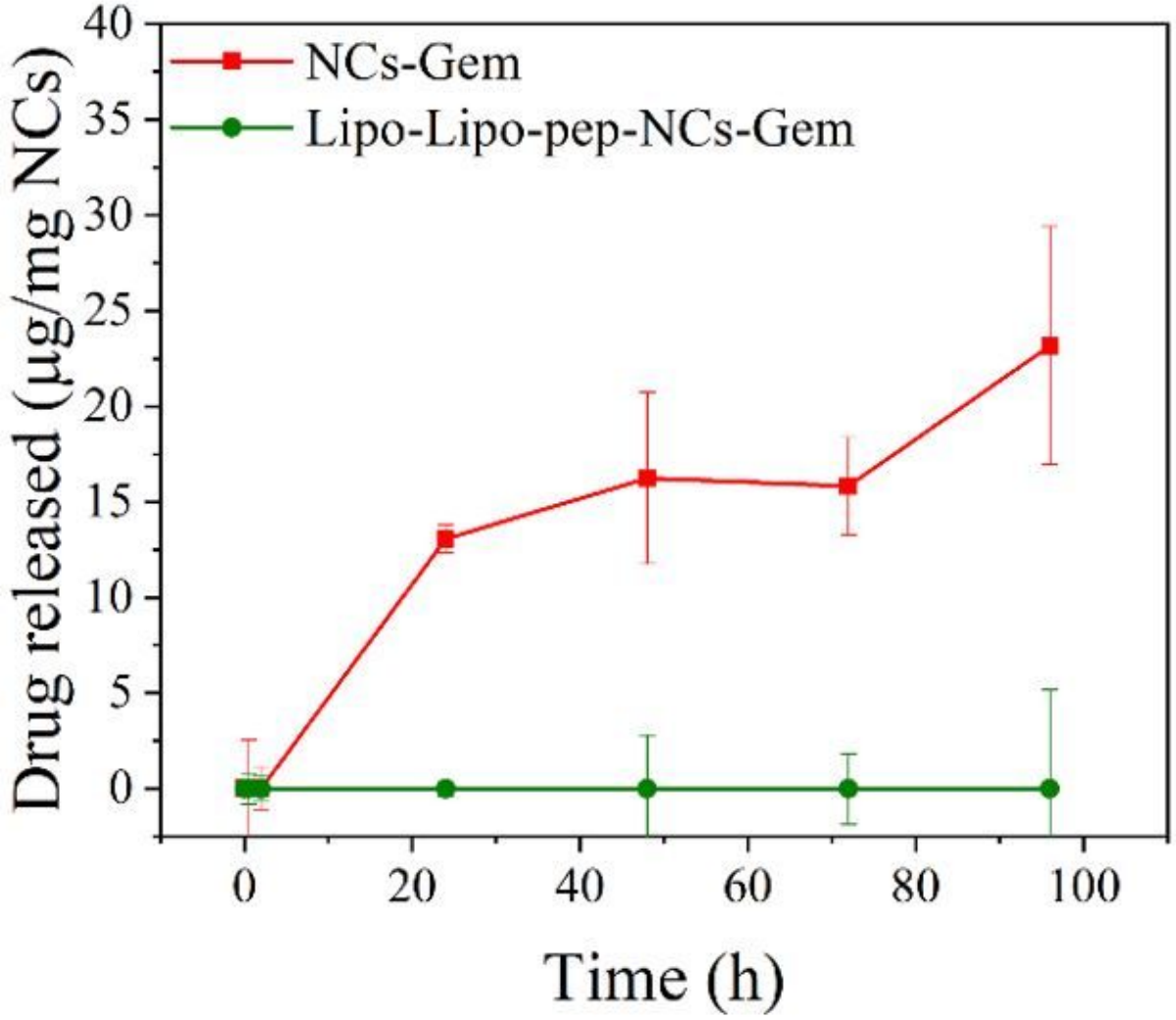

Figure 6

Gemcitabine release in RPMI up to 96 hours from functionalized Ol-ZnO-Gd NCs (here NCs, red line) and Lipo-Lipo-pep-NCs nanoconstruct (green line).

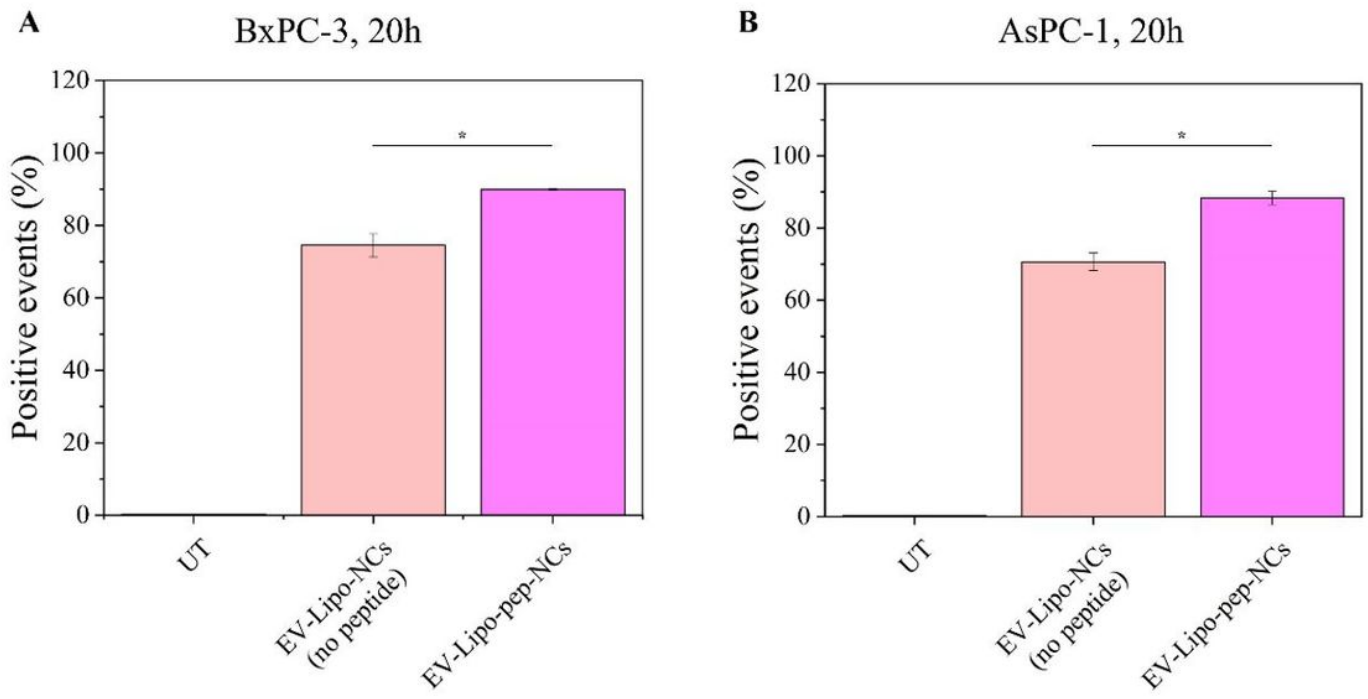

Figure 7

Comparison through flow cytometry analyses of the cellular uptake of the nanoconstruct without target peptide (pink bar) and with target peptide (violet bar) by (A) BxPC-3 and (B) AsPC-1 cells after 20 hours.

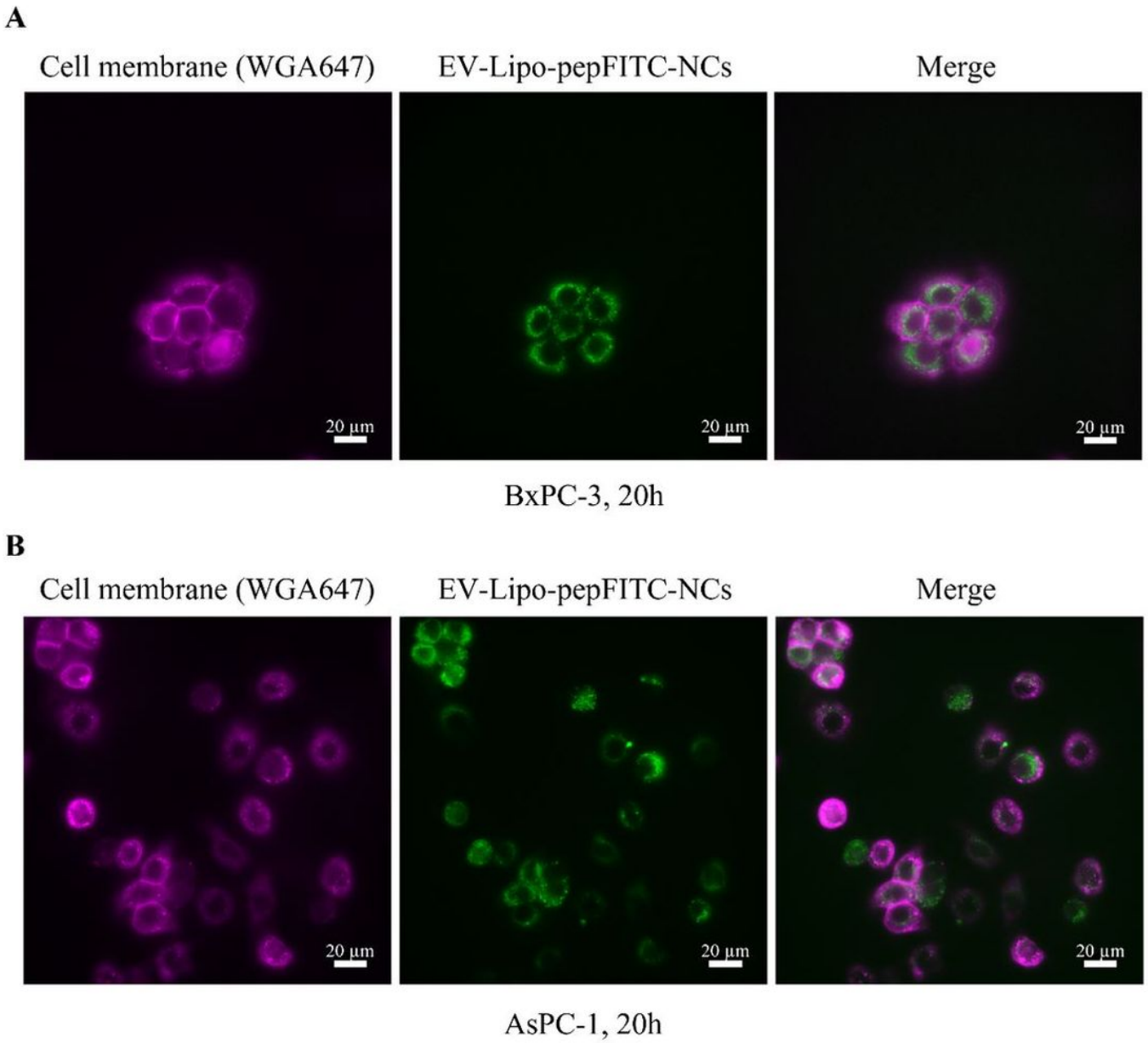

Figure 8

Cellular uptake analyses through fluorescence microscopy of the FITC-labeled EVs-Lipo-pep-NCs nanoconstruct by (A) BxPC-3 and (B) AsPC-1 cells after 20 hours; the cell membranes were labeled with WGA647. Scale bars: 20 μm.

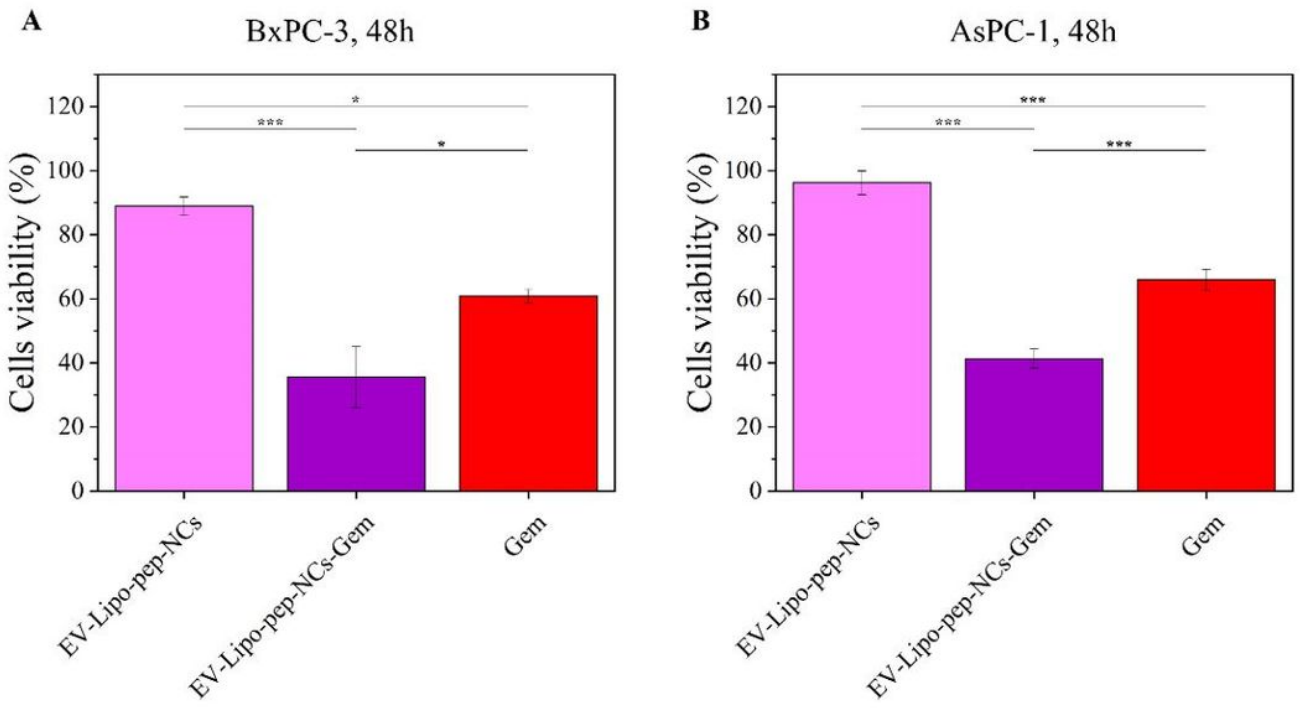

Figure 9

Cytotoxicity of the Gemcitabine-loaded EV-Lipo-pep-NCs nanoconstruct, compared to the nanoconstruct without drug and the free drug, on (A) BxPC-3 and (B) AsPC-1 cell lines after 48 hours.

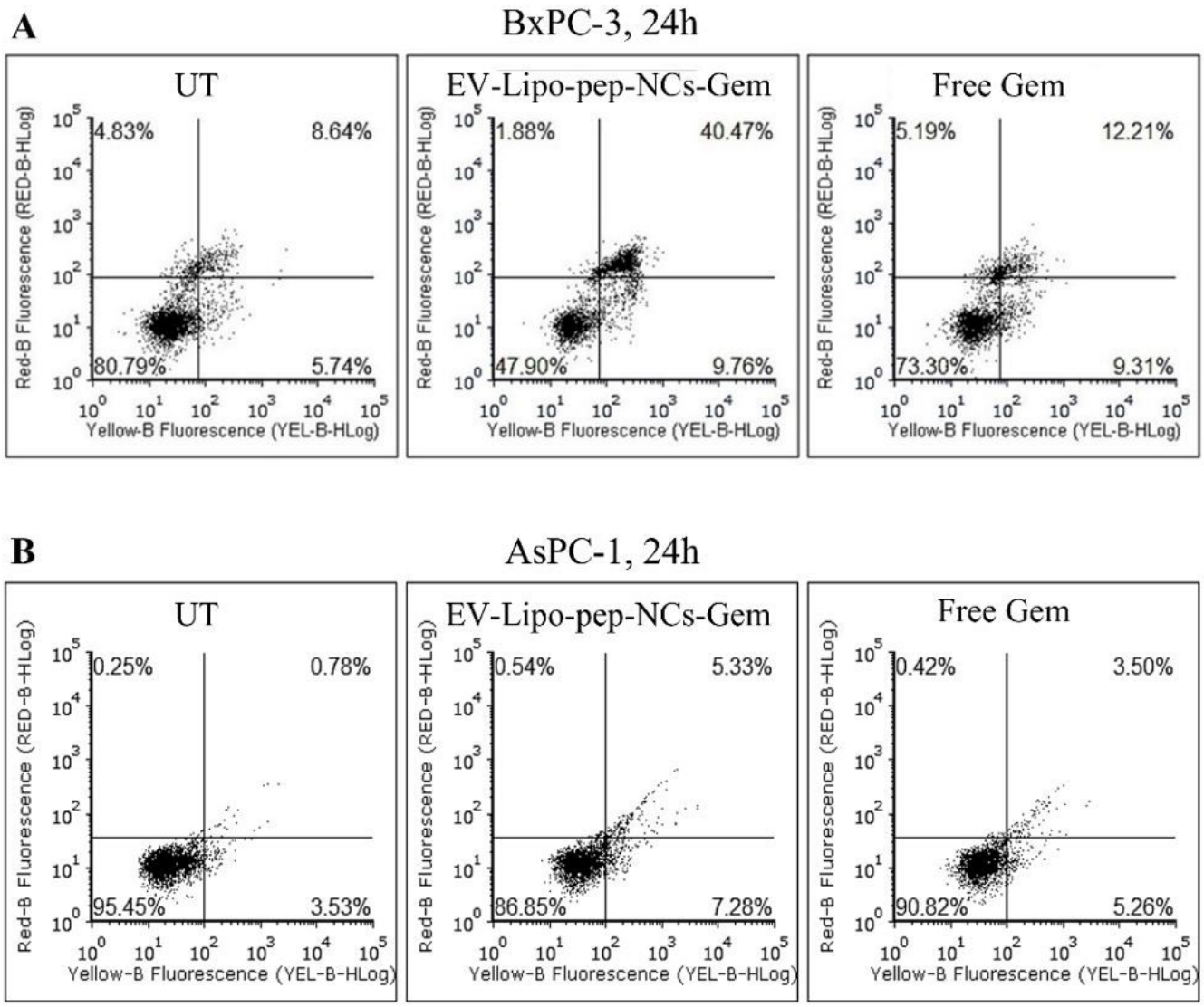

Figure 10

Dot plots of the apoptosis assay by flow cytometry on the BxPC-3 (A) and AsPC-1 (B) cells of the EV-Lipo-pep-NCs-Gem nanoconstruct (central panels), compared to the untreated cells (left side panels) and the free drug (right side panels).

Supplementary Files

This is a list of supplementary files associated with this preprint. Click to download.

- floatimage1.png